ARTICLE

3D-QSAR and Docking Studies of Pyrido[2,3-d]pyrimidine Derivatives as Wee1 Inhibitors

Guo-hua Zeng[a], Wen-juan Wu[a*], Rong Zhang[a], Jun Sun[a], Wen-guo Xie[a], Yong Shen[b]

a. Department of Physical Chemistry, Guangdong Pharmaceutical College, Guangzhou, 510006, China
b. School of Chemistry and Chemical Engineering, Sun Yat-Sen University, Guangzhou 510275, China

(Dated: Received on December 21, 2011; Accepted on February 20, 2012)

In order to investigate the inhibiting mechanism and obtain some helpful information for designing functional inhibitors against Wee1, three-dimensional quantitative structure-activity relationship (3D-QSAR) and docking studies have been performed on 45 pyrido[2,3-d] pyrimidine derivatives acting as Wee1 inhibitors. Two optimal 3D-QSAR models with significant statistical quality and satisfactory predictive ability were established, including the CoMFA model (q^2=0.707, R^2=0.964) and CoMSIA model (q^2=0.645, R^2=0.972). The external validation indicated that both CoMFA and CoMSIA models were quite robust and had high predictive power with the predictive correlation coefficient values of 0.707 and 0.794, essential parameter r_m^2 values of 0.792 and 0.826, the leave-one-out $r^2_{m(\mathrm{LOO})}$ values of 0.781 and 0.809, $r^2_{m(\mathrm{overall})}$ values of 0.787 and 0.810, respectively. Moreover, the appropriate binding orientations and conformations of these compounds interacting with Wee1 were revealed by the docking studies. Based on the CoMFA and CoMSIA contour maps and docking analyses, several key structural requirements of these compounds responsible for inhibitory activity were identified as follows: simultaneously introducing high electropositive groups to the substituents R1 and R5 may increase the activity, the substituent R2 should be smaller bulky and higher electronegative, moderate-size and strong electron-withdrawing groups for the substituent R3 is advantageous to the activity, but the substituent X should be medium-size and hydrophilic. These theoretical results help to understand the action mechanism and design novel potential Wee1 inhibitors.

Key words: Wee1, Pyrido[2,3-d]pyrimidine derivative, Three-dimensional quantitative structure-activity relationship, Docking study

I. INTRODUCTION

Many conventional anticancer therapies focus mainly on killing cells, regardless of whether they are healthy or cancerous. However, the combination of drugs that abrogate the G2/M checkpoint with a conventional DNA-damaging cytotoxic agent could be a promising method for cancer treatments [1−3]. It is well known that many cancer cells have defective G1 checkpoint mediated by p53 signaling pathway (which lacks the ability to repair DNA damage at a functional G1/S checkpoint) resulting in a dependence on the G2 checkpoint during cell replication [4]. However, cell cycle G2 checkpoint abrogation is more likely to affect cancer cells than normal ones. This checkpoint is mainly controlled by the two kinases: Wee1 and Chk1 [4]. And the former can not regulate the entry into mitosis by phosphorylating $p34^{cdc2}$ exclusively on Tyr15 [5]. Wee1 inhibitors can abrogate the G2/M checkpoint and preferentially boost the cytotoxic effects of DNA-damaging agents on p53-negative cells, meaning that the improvement could be achieved by using co-administration of a Wee1 inhibitor with a conventional DNA-damaging cytotoxic agent in the clinic [6−8]. On the basis of these findings, Wee1 has been recognized as an attractive therapeutic target for the discovery of antitumor drugs [9], and thus the development of novel Wee1-targeting agents is very significant.

In the past few years, a number of Wee1 inhibitors have been identified [10−12]. Parmer and coworkers synthesized a series of 4-phenylpyrrolocarbazole derivatives and assessed their anticancer activities in two human tumor cell lines: Wee1 and Chk1 [10]. Recently, pyrido[2,3-d]pyrimidine derivatives as potent Wee1 and Src inhibitors have also been reported [13] and some of them were found to sensitize p53 mutant cells to the DNA damage induced by radiation [14]. From the preliminary structure-activity relationship, we know that the peculiar chemical features may influence their activity. However, so far, the details on how the structure features of these compounds affect their anticancer ac-

*Author to whom correspondence should be addressed. E-mail: wuwenjuan83@126.com

tivities as well as the inhibitory mechanism of these compounds remain unknown. Thus, the investigation about the quantitative structure-activity relationship (QSAR) of this kind of compound undoubtedly enables us to gain an insight into the interaction mechanism and provides some useful information for designing new anticancer drugs.

QSAR methodology, which quantitatively describes the correlations between the variations in biological activity and the molecular structures or properties, is one of the most approaches for understanding the action mechanism of drugs and designing new drugs [15−17]. Nowadays, 3D-QSAR studies including comparative molecular field analysis (CoMFA) and comparative molecular similarity indices analysis (CoMSIA) have been successfully used in modern drug design [18−22]. In CoMFA, the biological activity of molecule is correlated with their steric and electrostatic interaction energies. However, CoMSIA refers to five molecular descriptors named steric, electrostatic, hydrophobic, hydrogen bond donor, and acceptor fields [23]. The 3D-QSAR models help to understand the nonbonding interaction characteristics between the drug molecule and the target protein, because they are vivid and robust. In addition, molecular docking is also a helpful approach which can simulate the interaction between a ligand and a receptor and thereby provide more insight into the interaction mechanism.

In this work, a series of Wee1 inhibitors, pyrido[2,3-d]pyrimidine derivatives, were selected to conduct 3D-QSAR and docking studies. To evaluate the predictive power of the constructed 3D-QSAR models, a systematic external validation was also employed. We focus on establishing optimal 3D-QSAR models and determining the probably binding conformations for these compounds, and expect the results can offer a theoretical direction for designing this kind of novel inhibitor with higher activity and some useful references for experimental work.

II. COMPUTATIONAL METHODS

A. Data set

A set of 45 variously functionalized pyrido[2,3-d] pyrimidine derivatives Wee1 inhibitors with well-expressed inhibitory activity [13] were used in this work (Table I). The common fragment of the studied compounds and the most active compound **35** (the atoms numbered from 1 to 25) are displayed in Fig.1. The total set of these compounds was divided into a training set (33 compounds) and a test set (12 compounds labeled with an asterisk in Table I). The test compounds were selected manually only in order to consider the structural diversity and wide range of activities in the data set. The IC_{50} values were converted to pIC_{50} ($-lgIC_{50}$) values and used as dependent variables in the CoMFA and CoMSIA calculations.

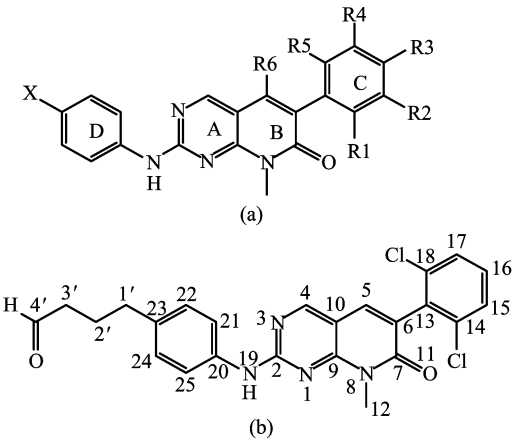

FIG. 1 Molecular structures of (a) pyrido[2,3-d]pyrimidine derivatives and (b) numbering of compound **35**.

B. Molecular docking

In order to identify the probable binding orientations and conformations of the studied derivatives interacting with Wee1, DOCK 6.0 program [24] was conducted to docking research for studied compounds. All parameters employed in docking were default unless otherwise stated.

The X-ray crystal structure of Wee1 taken from protein data bank (pdb Id: 1X8B) was employed to docking studies. At the beginning of docking, all the water molecules and subunits were removed, and hydrogen atoms and AMBER7FF99 charges were added to the protein. The Powell method in SYBYL 6.9 [25] was only used to minimize the energy of hydrogen atoms of protein in 1,000 cycles. The 3D structures of all studied Wee1 inhibitors were constructed in Chem3D software, energy minimizations were performed by semi-empirical quantum-chemical AM1 method. Then, all Wee1 inhibitors added with Gasteiger-Hückel charges were flexibly docked into the binding sites. The box size, grid space, energy cutoff distance, and maximum orientations were set as 6, 0.3, 12.0 Å, and 10^4, respectively.

C. Molecular modeling and alignment

CoMFA and CoMSIA models were generated by using molecular modeling software package SYBYL 6.9 [25] running on an SGI R2400 workstation. All parameters used in CoMFA and CoMSIA were default except for explained.

Selecting the suitable active conformation is a key step for CoMFA and CoMSIA analyses. The accuracy and reliability of CoMFA and CoMSIA models are also

DOI:10.1088/1674-0068/25/03/297-307

TABLE I Molecular structures of compounds and their Wee1 inhibitory activities.

No.	R1	R2	R3	R4	R5	R6	X	IC_{50}/(μmol/L)
1*	Cl	H	H	H	Cl	H	H	2.6
2	F	H	H	H	F	H	H	9.7
3*	Br	H	H	H	Br	H	H	0.41
4	Me	H	H	H	Me	H	H	0.99
5	CF_3	H	H	H	CF_3	H	H	41
6	OH	H	H	H	OH	H	H	27
7	Cl	H	H	H	F	H	H	2.4
8*	Cl	H	H	H	Me	H	H	1.9
9*	Cl	H	H	H	OMe	H	H	3.4
10	Cl	H	H	H	OH	H	H	1.5
11	Me	H	H	H	Br	H	H	4.5
12*	OMe	H	H	H	OH	H	H	11
13	Cl	CH_2OH	H	H	H	H	H	3.5
14	Cl	CH_2NH_2	H	H	H	H	H	31
15	Cl	CO_2H	H	H	H	H	H	3.2
16	Cl	$CONH_2$	H	H	H	H	H	8.6
17	Cl	OH	H	H	H	H	H	0.074
18	Cl	NH_2	H	H	H	H	H	2.6
19	Cl	H	OH	H	H	H	H	0.22
20	Me	H	OH	H	H	H	H	0.58
21*	Cl	H	NH_2	H	H	H	H	3.7
22	Cl	H	NHAc	H	H	H	H	36
23	Cl	OH	H	OH	H	H	H	0.14
24	Me	OMe	H	OMe	H	H	H	33
25	Me	OH	H	OH	H	H	H	1
26	Cl	H	H	H	H	H	CH_2CONH_2	0.12
27*	Cl	H	H	H	H	H	$(CH_2)_2CONH_2$	0.19
28	Cl	H	H	H	H	H	$(CH_2)_4CONH_2$	0.26
29*	Cl	H	H	H	H	H	OCH_2CONH_2	0.25
30	Cl	H	H	H	H	H	$O(CH_2)_2NEt_2$	0.99
31	Cl	H	H	H	H	H	$O(CH_2)_3CO_2H$	0.086
32*	Cl	H	H	H	H	H	$(CH_2)_3CO_2(CH_2)_2$Nmorph	0.095
33	Cl	H	H	H	H	H	$(CH_2)_3CO_2(CH_2)_2NMe_2$	0.124
34*	Cl	H	H	H	H	H	$(CH_2)_3CO_2(CH_2)_2$Npip	0.142
35	Cl	H	H	H	H	H	$(CH_2)_3CO_2H$	0.032
36	Cl	H	H	H	H	H	$CH_2CH(NH_2)CO_2H$	0.09
37	Cl	H	H	H	H	H	$(CH_2)_3$tetrazole	0.069
38*	Cl	OH	H	H	H	H	$O(CH_2)_2NEt_2$	0.15
39	Cl	OH	H	H	H	H	$O(CH_2)_2CO_2H$	0.04
40	Cl	H	OH	H	H	H	$O(CH_2)_2NEt_2$	0.08
41	Cl	H	OH	H	H	H	$O(CH_2)_3CO_2H$	0.04
42*	Me	H	H	H	Me	Me	H	0.41
43	Me	H	H	H	Me	Me	$O(CH_2)_2NEt_2$	0.55
44	Cl	H	H	H	H	Me	H	1.2
45	Cl	H	H	H	H	Me	$O(CH_2)_2NEt_2$	0.54

* Compounds in the test set.

DOI:10.1088/1674-0068/25/03/297-307

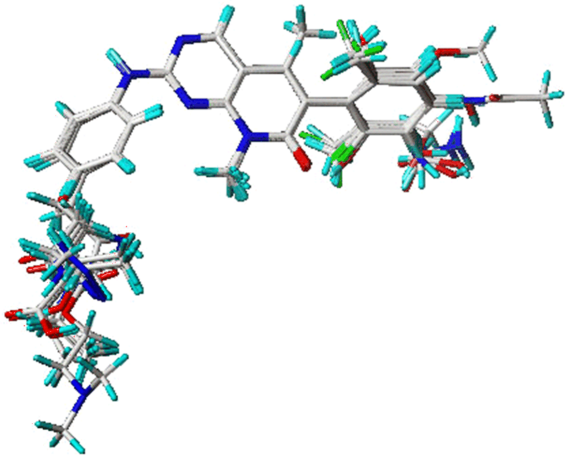

FIG. 2 Superposition of the 33 studied compounds.

directly dependent on the rule of the ligand alignment [26]. Since the crystal structure of complex of Wee1 with one of these compounds is not available, conformation search was performed using Chem3D software [27] to find out the global energy-minimum conformation for the most active compound **35** by rotating rotatable bonds. Afterwards, the active conformation with minimum energy was further optimized by the Gaussian 03 program package [28] using semi-empirical quantum-chemical AM1 calculations. The rest of molecules were built by changing the substitutions of compound **35** and minimized with the same way. The most active compound **35** was used as a template for aligning the rest of molecules to it. The aligned compounds are displayed in Fig.2.

D. CoMFA and CoMSIA studies

Models of steric and electrostatic fields for CoMFA were based on both Lennard-Jones and Coulombic potentials [29]. The steric and electrostatic interactions were calculated using Tripos force field with a distance dependent-dielectric constant at all intersections in a regular spaced (2 Å) grid taking a sp^3 carbon atom as steric probe and a +1 charge as electrostatic probe. The truncation for both the steric and the electrostatic energies were set to 125.4 kJ/mol. To improve the signal-to-noise ratio, the minimum sigma (column filtering) was set to 8.4 kJ/mol by omitting those lattice points whose energy variation was below this threshold.

The CoMSIA method defines explicit hydrophobic, hydrogen bond donor, and acceptor fields in addition to the steric and electrostatic fields used in CoMFA. The CoMSIA [30] similarity index descriptors were obtained using the same lattice boxes as those used in CoMFA calculations. A sp^3 carbon probe atom with a charge of +1.0, a radius of 1.0 Å, hydrophobicity of +1.0, and H-bond donor and acceptor properties of +1 were employed to calculate the respective fields. A Gaussian-type functional form is adopted to evaluate the mutual distance between the probe atom and each molecule atom. The attenuation factor α was set to 0.3.

E. Partial least squares analysis and validation of QSAR models

The 3D-QSAR models were derived using the partial least-square (PLS) statistical method [31, 32] which was used to construct a linear correlation between the CoMFA/CoMSIA fields (independent variables) and the inhibitory activity values (dependent variables). In order to select the optimal model, the cross-validation analysis was performed with the leave-one-out (LOO) method in which one compound was removed from the data set and its activity was predicted using the model built from the rest of the data set. It yields the highest cross-validated correlation coefficient (q^2) and the optimum number of components N. The non-cross-validation methods were appraised by the conventional correlation coefficient R^2, standard error of estimates (SEE), and the Fisher ratio value F. To further validate the derived models, bootstrapping analysis for 100 runs was also performed.

To assess the validity of QSAR models generated from the training set, the biological activities of 12 compounds in the external test set will be predicted. The predictive power of the models is judged based on the predictive correlation coefficient $R^2_{\rm pred}$ calculated by the following equation [33−37]:

$$R^2_{\rm pred} = 1 - \frac{\sum \left(Y_{\rm pred(Test)} - Y_{\rm Test}\right)^2}{\sum \left(Y_{\rm Test} - Y_{\rm training}\right)^2} \tag{1}$$

In the above equation, $Y_{\rm pred(Test)}$ and $Y_{\rm Test}$ indicate predicted and observed activity values of the test set compounds, respectively. $Y_{\rm training}$ indicates mean activity values of the training set. However, in many cases, the $R^2_{\rm pred}$ value may not be regarded as the only criterion to indicate the external predictability of a QSAR model [38]. Hence, further external validation is required. Globraikh and Tropsha have suggested that for an ideal model

$$\begin{aligned} Y_{\rm pred(Test)} &= aY_{\rm Test} + b \\ &= kY_{\rm Test} \end{aligned} \tag{2}$$

slope a should be equal to 1, intercept b should be equal to 0, and slope k through the origin should be close to 1 [39].

In addition, according to Roy [38], another essential parameter r^2_m is calculated as follow:

$$r^2_m = r^2\left(1 - \sqrt{|r^2 - r^2_0|}\right) \tag{3}$$

DOI:10.1088/1674-0068/25/03/297-307

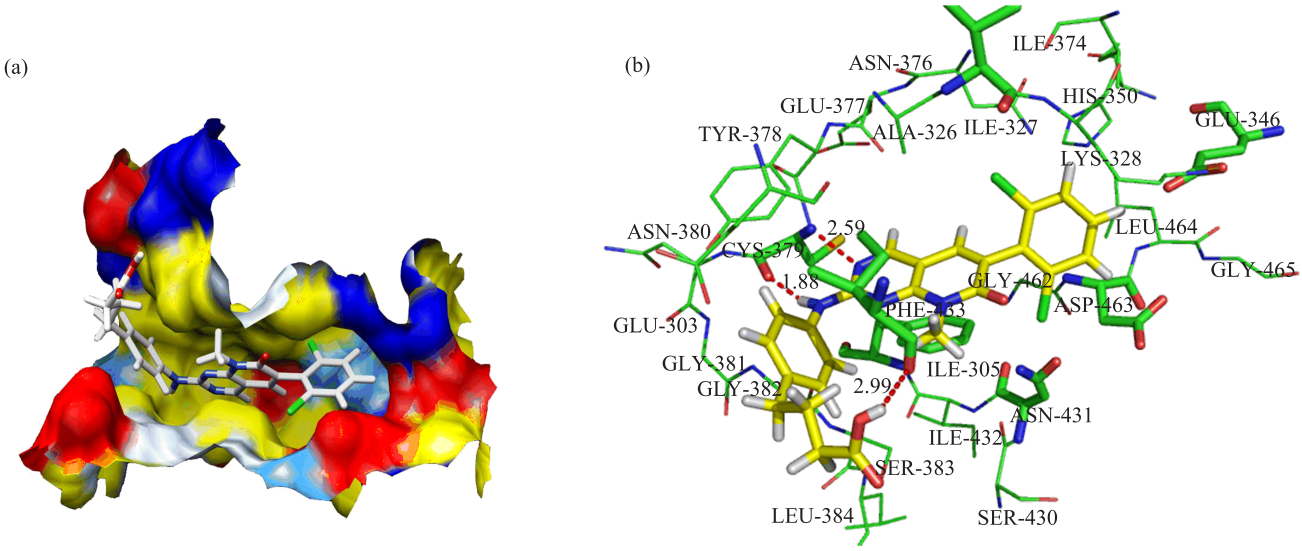

FIG. 3 (a) Docking structure of the most potent compound **35** and corresponding surface of Wee1 at the ATP-binding site, in which red areas represent electrostatic potential, blue areas denote positive potential, yellow areas represent hydrophobic potential, hydrophilic regions are in white, neutral areas are in light cyan. (b) Interactions between the ATP-binding site and compound **35**. Hydrogen bonds are depicted as red dotted lines. For interpretation of the color in this figure legend, the reader can refer to the web version of this article.

where r^2 and r_0^2 are squared correlation coefficient values between observed and predicted values of the test set compounds with and without intercept. For a model with good external predictability, the r_m^2 value should be greater than 0.5. In summary, a 3D-QSAR model is considered to be acceptable if it satisfies all of the following conditions: R^2>0.6, q^2>0.5, $[(r^2-r_0^2)/r^2]$<0.1, 0.85≤k≤1.15, and r_m^2>0.5. Nonetheless, the parameter r_m^2 is only applied to the test set, so we also calculated another two additional validation parameters: $r_{m(\mathrm{LOO})}^2$ using for the training set and $r_{m(\mathrm{overall})}^2$ using for the whole set.

III. RESULTS AND DISCUSSION

A. Validation of docking reliability

Before docking pyrido[2,3-d]pyrimidine derivatives into the Wee1 binding site, the reliability of the docking project should be first validated. We adopted the known X-ray structure of Wee1 in complex with the molecular ligand 824 to perform the validation. The ligand 824 was flexibly redocked into the binding site of Wee1 kinase and the docking conformation corresponding to the lowest energy score was selected as the most probable binding conformation. The root-mean-square deviation (RMSD) between the conformation of crystallographic 824 and redocked 824 was 0.29 Å, suggesting the parameter set for the docking simulation was reasonable to reproduce the X-ray structure. Thus, this docking method and the used parameters set can be extended to find the binding conformations of other Wee1 inhibitors.

B. Docking results

All studied inhibitors were docked into the binding site of Wee1 kinase. The poses of all the studied compounds had similar binding positions and orientations with each other and with the crystallized inhibitor. To explore the detailed binding characteristics of these compounds, the most active compound **35** was selected to perform the deeper docking study and its binding model with Wee1 kinase was constructed and showed in Fig.3. Compound **35** is suitably situated at the ATP-binding site, resulting in various interactions with the hinge-binding region of the enzyme.

The ring-C is surrounded by the side chains of Ile327, Lys328, Glu346, His350, Ile374, Asn431, Gly462, Asp463, Leu464, and Gly465. It also forms π-cation interactions with the NH_3^+ groups of Lys328 and His350. The substituent X of ring-D at the entrance of the ATP-binding pocket created by Glu303, Asp380, Gly381, Gly382, Ser383, and Leu384 is placed in the solvent accessible region. The N3 and N19 atoms of pyridine ring simultaneously have H-bonds interactions with backbone atoms of Cys379. Another hydrogen bond is formed between H atom of the hydroxyl of 4′-position on substituent X and the carbonyl of Ile305. Meanwhile, π-π stacking between the pyridine ring and Phe433 could be easily found.

C. CoMFA and CoMSIA analyses

The 3D-QSAR models were generated from CoMFA and CoMSIA analyses and their statistical parameters are listed in Table II. For a reliable predictive model,

DOI:10.1088/1674-0068/25/03/297-307

TABLE II CoMFA and CoMSIA PLS results.

		R^2	N	q^2	SEE	F	$R^2_{\rm bs}$	$SD_{\rm bs}$
CoMFA	SE	0.964	6	0.708	0.204	117.580	0.977	0.114
CoMSIA	SED	0.954	3	0.584	0.230	90.718	0.977	0.162
	EHD	0.969	3	0.620	0.190	136.195	0.983	0.136
	SEHD	0.972	3	0.645	0.181	148.955	0.984	0.131
	SEHA	0.971	6	0.575	0.185	143.565	0.980	0.148
	EHDA	0.968	5	0.603	0.193	131.047	0.980	0.145
	SEHDA	0.966	5	0.619	0.198	124.904	0.982	0.144

N is the optimal number of components, q^2 is the square of leave-one-out (LOO) cross-validation coefficient, R^2 is the square of non-cross-validation coefficient, SEE is the standard error of estimation, F is the F-test value, $R^2_{\rm bs}$ is the square of R bootstrapping analysis (100 runs), $SD_{\rm bs}$ is the mean standard deviation by bootstrapping analysis. S, E, H, D, and A represent the steric, electrostatic, hydrophobic, hydrogen-bond donor, and acceptor fields, respectively.

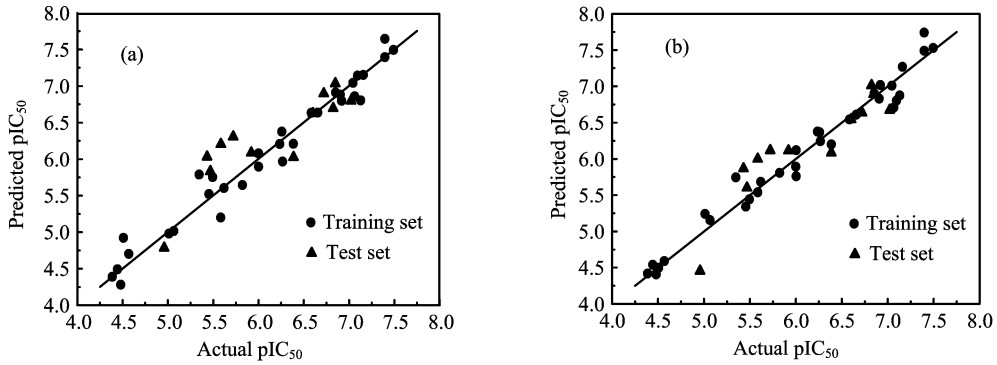

FIG. 4 Plots of predicted activities *vs.* actual ones for (a) CoMFA and (b) CoMSIA (SEHD) analyses.

the cross-validated coefficient q^2 should be greater than 0.5.

This CoMFA model has high R^2 (0.964), F (117.580), q^2 (0.708), as well as small SEE (0.204), indicating that the established CoMFA model is reliable and acceptable for these compounds. Moreover, the $R^2_{\rm bs}$ of 0.977 and $SD_{\rm bs}$ of 0.114 obtained from bootstrapping analysis (100 runs) further verify the statistical validity and robustness of the derived CoMFA model. The contributions of steric and electrostatic fields were 61.8% and 38.2%, respectively. Therefore, the steric field has a greater influence than the electrostatic field, indicating that the steric interaction of the inhibitor with the receptor could be a more significant factor for the Wee1 inhibitory activity.

The PLS results of CoMSIA analysis using different combinations of steric (S), electrostatic (E), hydrophobic (H), hydrogen bond donor (D), and acceptor (A) fields are also summarized in Table II. As shown in Table II, these six CoMSIA models all show good correlative and predictive ability, in which steric, electrostatic, hydrophobic, and hydrogen bond donor fields were observed to be predominant over hydrogen bond acceptor fields. The CoMSIA (SEHD) model gives R^2 of 0.972, q^2 of 0.645, F of 148.955, $R^2_{\rm bs}$ of 0.984, indicating that this model is reliable and able to predict inhibitory activities of new Wee1 inhibitors. The contributions of steric, electrostatic, hydrophobic, and hydrogen bond donor fields were 0.101, 0.316, 0.223, and 0.360, respectively.

The predicted $\rm pIC_{50}$ values of the training and test sets are listed in Table III. The plots of the predicted $\rm pIC_{50}$ values versus the actual ones for the CoMFA and CoMSIA (SEHD) analyses are depicted in Fig.4, where most points are evenly distributed along the line $Y=X$, implying that these two models are of good quality.

D. External validation for CoMFA and CoMSIA models

A reliable QSAR model should be able to accurately predict activities of new compounds. The high q^2 (0.708) in the above-mentioned training set only shows good internal validation, but it does not automatically infer its high predictive ability for an external test set [40]. To derive a QSAR model with well-accepted predictive ability, external validation is also necessary. Thus, the established CoMFA and CoMSIA (SEHD) models were further exploited to predict the activities of 12 compounds (Table III) as an external test set and several statistical parameters like $R^2_{\rm pred}$, k, r^2_m, $r^2_{m(\rm LOO)}$, and $r^2_{m(\rm overall)}$ were employed. According to the above-

DOI:10.1088/1674-0068/25/03/297-307

TABLE III The actual pIC_{50}, predicted pIC_{50} and their residuals of the studied compounds for CoMFA and CoMSIA(SEHD).

		CoMFA		CoMSIA(SEHD)				CoMFA		CoMSIA(SEHD)	
Compound	Actual pIC_{50}	Pred.	Res.[a]	Pred.	Res.	Compound	Actual pIC_{50}	Pred.	Res.[a]	Pred.	Res.
	Training set						Training set				
2	5.013	4.984	0.029	5.241	−0.228	**33**	6.907	6.890	0.017	6.830	0.077
4	6.004	5.901	0.103	5.759	0.245	**35**	7.495	7.504	−0.009	7.527	−0.032
5	4.387	4.390	−0.003	4.420	−0.033	**36**	7.046	7.053	−0.007	7.010	0.036
6	4.569	4.704	−0.135	4.590	−0.021	**37**	7.161	7.160	0.001	7.268	−0.107
7	5.620	5.609	0.011	5.684	−0.064	**39**	7.398	7.657	−0.259	7.742	−0.344
10	5.824	5.649	0.175	5.807	0.017	**40**	7.097	7.152	−0.055	6.804	0.293
11	5.347	5.792	−0.445	5.745	−0.398	**41**	7.398	7.405	−0.007	7.490	−0.092
13	5.456	5.525	−0.069	5.342	0.114	**43**	6.268	5.972	0.296	6.242	0.026
14	4.509	4.923	−0.414	4.499	0.010	**44**	6.387	6.215	0.172	6.199	0.188
15	5.495	5.759	−0.264	5.440	0.055	**45**	6.260	6.384	−0.124	6.367	−0.107
16	5.066	5.017	0.049	5.155	−0.089		Test set				
17	7.131	6.810	0.321	6.873	0.258	**1**	5.585	6.203	−0.618	6.000	−0.415
18	5.585	5.203	0.382	5.540	0.045	**3**	6.387	6.025	0.362	6.084	0.303
19	6.658	6.644	0.014	6.610	0.048	**8**	5.721	6.307	−0.586	6.115	−0.394
20	6.237	6.213	0.024	6.376	−0.139	**9**	5.469	5.832	−0.363	5.600	−0.131
22	4.444	4.493	−0.049	4.539	−0.095	**12**	4.959	4.785	0.174	4.455	0.504
23	6.854	6.919	−0.065	6.904	−0.050	**23**	5.432	6.032	−0.600	5.865	−0.433
24	4.481	4.282	0.199	4.406	0.075	**29**	6.721	6.898	−0.177	6.636	0.085
25	6.000	6.085	−0.085	5.893	0.107	**31**	6.602	6.626	−0.024	6.543	0.059
26	6.921	6.806	0.115	7.018	−0.097	**34**	7.022	6.797	0.225	6.674	0.348
28	6.585	6.642	−0.057	6.545	0.040	**36**	6.848	7.034	−0.186	6.891	−0.043
30	6.004	6.083	−0.079	6.119	−0.115	**40**	6.824	6.694	0.130	7.013	−0.189
31	7.066	6.868	0.198	6.706	0.360	**44**	5.921	6.087	−0.166	6.114	−0.193

[a] Residual=pIC_{50} (Act.)−pIC_{50} (pred.).

mentioned method of validating an ideal model, a 3D-QSAR model is acceptable if it satisfies all of the following conditions: R^2>0.6, q^2>0.5, $[(r^2-r_0^2)/r^2]$<0.1, 0.85≤k≤1.15, and r_m^2>0.5.

The established CoMFA model was employed to predict activities of 12 compounds in the test set, resulting in satisfactory statistical parameters: R^2_{pred}=0.707, r^2=0.931, r_0^2=0.932, $[(r^2-r_0^2)/r^2]$=0.033, k=0.976 (Fig.5(a)). These parameters quite accord with the above criteria. Moreover, the additional external validation parameters value r_m^2 reaches 0.792, the train set validation value $r^2_{m(\text{LOO})}$ reaches 0.781 (Fig.5(b)), and the whole set validation value $r^2_{m(\text{overall})}$ reaches 0.787 (Fig.5(c)), respectively.

Similarly, further external validation was carried out to evaluate the various CoMSIA models. The CoMSIA(SEHD), CoMSIA(SEHDA), and CoMSIA(EHDA) models exhibit advantageous results in the external validation. However, the CoMSIA(SEHD) model was slightly better than the CoMSIA(SEHDA) and CoMSIA(EHDA) models. Therefore, the CoMSIA(SEHD) model was selected as the best model for further discussion. It gives the statistically validating results with R^2_{pred} of 0.794, r^2=0.957, r_0^2=0.979, $[(r^2-r_0^2)/r^2]$=−0.023, k of 0.992 (0.85≤k≤1.15), r_m^2 of 0.826 (>0.5), $r^2_{m(\text{LOO})}$ of 0.809, and $r^2_{m(\text{overall})}$ of 0.810.

In short, all of the statistical and validating parameters show that the derived CoMFA and CoMSIA(SEHD) models all exhibit the satisfactory predictive ability. The results of the external validation for both models are depicted in Table IV.

E. Graphical interpretation of the results

CoMFA and CoMSIA models can be displayed as vivid 3D contour maps (Fig.6), which can provide a more exhaustive interpretation of the biological activity and the related molecular region information. The steric interactions are represented by green and yellow contours, green contours indicate the regions with bulky groups would be favorable, whereas yellow contours show the regions with bulky substituents would decrease the activity. The electrostatic interactions are represented by red and blue contours, red contours show

DOI:10.1088/1674-0068/25/03/297-307

TABLE IV Summary of external validation results of CoMFA and CoMSIA analyses.

		$R^2_{\rm pred}$	Slope k	$(r^2-r_0^2)/r^2$	r_m^2	$r^2_{m(\rm LOO)}$	$r^2_{m(\rm overall)}$
CoMFA	SE	0.707	0.976	0.033	0.792	0.781	0.787
CoMSIA	SED	0.737	1.006	−0.033	0.755	0.749	0.750
	EHD	0.781	0.997	−0.031	0.801	0.798	0.799
	SEHD	0.794	0.992	−0.023	0.826	0.809	0.810
	SEHA	0.755	0.986	−0.011	0.872	0.806	0.808
	EHDA	0.806	0.994	−0.029	0.804	0.795	0.795
	SEHDA	0.795	0.995	−0.034	0.792	0.788	0.788

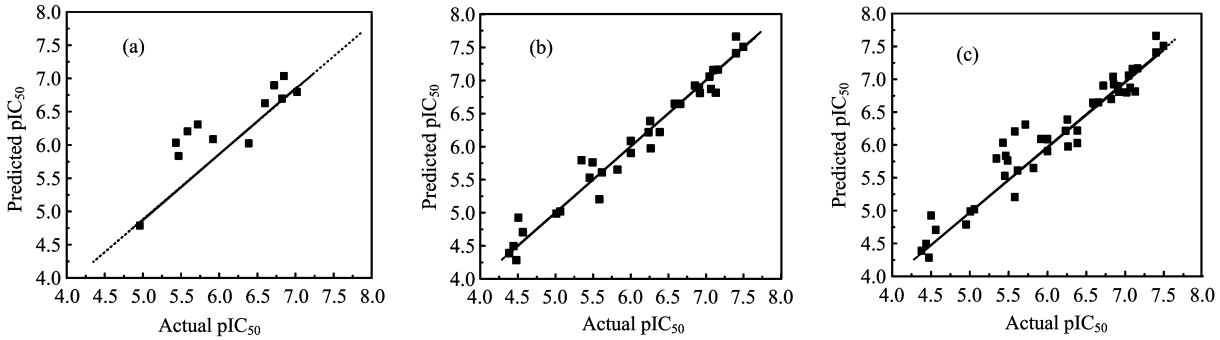

FIG. 5 (a) A regression of actual *vs.* predicted activities for 12 compounds from the external test set. (b) A regression of actual activities *vs.* LOO predicted activities for 33 compounds from the training set in the CoMFA model. (c) A regression of actual activities *vs.* predicted activities for 45 compounds from the whole set. The solid lines are not through the origin and the black dots are through the origin.

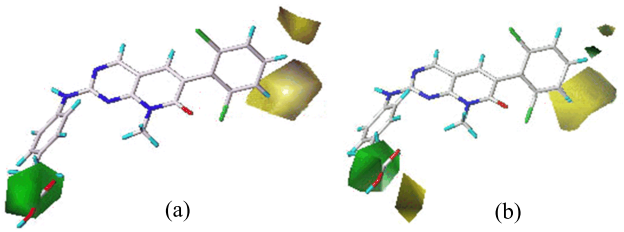

FIG. 6 Steric contour maps of the most active compound 35 for (a) CoMFA and (b) CoMSIA(SEHD).

favorable electronegative regions, while blue contours indicate the regions where electropositive groups would be favorable to the activity. In hydrophobic contours, yellow contours represent hydrophobically favored regions and white contours represent hydrophilically favored regions. In hydrogen bond donor contours, cyan color is favorable to the activity while purple color is unfavorable to the activity. In hydrogen bond acceptor contours, magenta color is favorable to the activity and red color is unfavorable to the activity.

The calculated CoMFA and CoMSIA(SEHD) steric contour maps are displayed in Fig.6, using compound **35** as a reference structure. As shown in Fig.6(a), a large yellow contour region embedding in substituent R2 of ring-C shows that introducing bulky groups in this position of substituent R2 would be unfavorable, because it can be blocked by the side chain of the nearest residue Asp463. For instance, compounds **17** (7.131) and **18** (5.585) have −OH and $-NH_2$, respectively. They exhibit higher activities than corresponding compounds **13** (5.456), **14** (4.509), **15** (5.495), and **16** (5.066) which possess relatively larger $-CH_2OH$, $-CH_2NH_2$, $-CO_2H$, and $-CONH_2$ groups, respectively. And a relatively small yellow contour region is found at some distance from substituent R3, which is blocked by the side chain of Glu346, demonstrating that bulky substituents around this region would decrease the activity. This can explain well why compound **22** (4.444) with −NHAc as substituent R3 shows worse potency than compounds **19** (6.658) and **21** (5.432) with −OH and $-NH_2$, respectively, at the same site. Moreover, there is a big green contour embedding the region between the 3′- and 4′- positions of X group, indicating that bulky groups at this site are highly desirable for improved inhibitory potency. This may be the reason why compounds **26**−**41**, **43**, and **45** with bulky groups (*e.g.* $(CH_2)_3COOH$, $(CH_2)_3$tetrazole) as substituent X exhibit more significantly improved activities than those compounds **1**, **2**, **4**−**16**, **18**, **19**, **21**, **22**, **24**, **25**, and **44** without substituent X. The steric contour map of CoMSIA(SEHD) (Fig.6(b)) is quite similar to that of CoMFA except for some small differences. It is notable that a small green contour inserting one small yellow contour is near substituent R3, indicating that moderate-size groups in this green posi-

DOI:10.1088/1674-0068/25/03/297-307

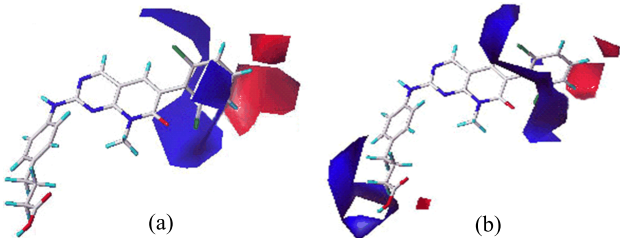

FIG. 7 Electrostatic contour maps of the most active compound **35** for (a) CoMFA and (b) CoMSIA(SEHD).

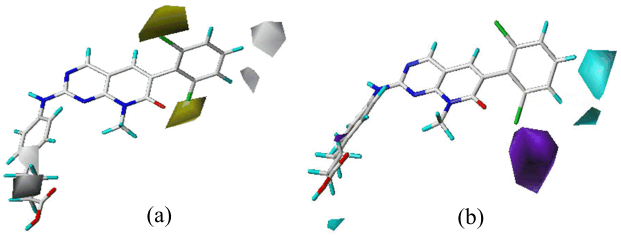

FIG. 8 (a) CoMSIA(SEHD) hydrophobic contour map and (b) CoMSIA(SEHD) hydrogen bond donor map for the most active of compound **35**.

tion would enhance the inhibitory activity. Compounds **19** (6.658) and **21** (5.432) with a moderate-size group $-OH$ or $-NH_2$ as substituent R3 both have higher activities compared with compound **22** (4.444), because compound **22** has a relatively bulky $-NHAc$ group just falling into the yellow region. In addition, it is also observed that there is a small yellow contour far away from X group, suggesting that an overlarge-size substituent X would be unfavorable to the activity. Compounds **32** (7.022), **33** (6.907), and **34** (6.848) display lower activities than compound **35** (7.495), because compounds **32**, **33**, and **34** all have overlarge-size groups as substituent X just reaching the yellow region.

The electrostatic contour maps of CoMFA and CoMSIA(SEHD) are displayed in Fig.7. There are three blue contours near substituents R1 and R5 of the template molecule, suggesting that the presence of strong electropositive or weak electronegative groups on these positions would be favorable to the activity. The docking study showed that the nearest residues toward substituents R1 and R5 are Asn431 and Ile327, respectively, which may not be interacted well with R1 and R5 bearing strong electronegativity. For instance, compared compounds **2** (5.013) with **7** (5.62), **4** (6.004) with **8** (5.721), as well as **6** (4.569) with **10** (5.824), their discrepancies in activity can be interpreted by these blue contours. Similarly, compound **8** (5.721) with $-CH_3$ as substituent R5 shows better potency than compound **1** (5.585) with $-Cl$ on this site. Compounds **3** (6.387), **1** (5.585), and **2** (5.013) have an order for the activity of **3**>**1**>**2** with the corresponding $-Br$, $-Cl$, $-F$ as substituents R1 and R5, respectively. In addition, two red regions are near substituents R2 and R3 in the Fig.7(a), indicating that electron-withdrawing substituents around these positions would be favored. The docking study also showed that the nearest residues are Glu346 and Asp463, which can form H-bonds with electron-rich O atom of substituent R2 and electron-rich N atom of substituent R3, respectively. This may be the reason why compounds **38** (6.824), **39** (7.398), **40** (7.097), and **41** (7.398) with $-OH$ or $-NH_2$ are highly active. Electronegative substituents like $-OH$ or $-NH_2$ at the R2 and R3 positions could form H-bond interaction with Glu346 and Asp463. On the contrary the compounds **30** (6.004) and **31** (7.066) with H atom are less active. The electrostatic contour map of CoMSIA(SEHD) (Fig.7(b)) is similar to that of CoMFA except for the large blue polyhedron around the 1′-, 2′-, 3′-positions of X group and a small red contour at the terminal of substituent X. The former indicates that electron-donating atoms at these sites would be favorable. For example, compounds **27** (6.721) and **35** (7.495) both with C atom as the first atom of substituent X display higher activities than compounds **29** (6.602) and **31** (7.066) both with stronger electronegative O atom as the first atom of X group. The small red contour at the terminal of substituent X suggests that the introduction of high electronegative group at this site could boost the activity. Compounds **33** (6.907) and **34** (6.848) are observed with lower activities than compound **32** (7.022), because the terminal of substituent X of the latter is morpholine ring in which O atom with greater electronegativity just falls into the red region.

The hydrophobic contour map is displayed in Fig.8(a). Two large yellow contours near substituents R1 and R5 indicate that hydrophobic groups at these sites would benefit the activity. This is in agreement with the above result that low electronegative groups around these positions are advantageous to improving the activity, since usually weak electronegative groups are relatively hydrophobic. There are two white contours around ring-C. One is near substituent R2 of the template molecule, and another one is near the substituent R3, indicating that hydrophilic substituents are well tolerated in these regions. This is compatible with the above result that strong electronegative groups as substituents R2 and R3 are advantageous to improving the inhibitory activity, since high electronegative groups usually exhibit relatively hydrophilicity. Additionally, two relatively small white contours embedding the substituent X, suggesting that substituent X with hydrophilic character prefers this position. As shown in Fig.3(a), it is observed that substituent X stretches outside the entrance of the binding groove of Wee1 kinase, suggesting that bulky substituents with moderate length could be tolerated by enzyme. Moreover, substituent X is exposed to the solvent area and the substituent X with hydrophilic atoms should have some good physicochemical properties, such as solubil-

DOI:10.1088/1674-0068/25/03/297-307

ity, permeability, *etc.*, to increase the binding ability to plasma protein. For example, most of the excellent compounds (**26**−**29**, **31**−**41**) all possess a relatively hydrophilic group as substituent X, whereas those without a relatively hydrophilic group as substituent X exhibit relatively weaker activity (**1**−**16**, **18**, **20**−**22**, **24**, **25**, **42**, **44**). Meanwhile, this is a possible reason why compounds **26** (6.921), **43** (6.268), **39** (7.398), and **40** (7.097) with moderate-size substituent X have higher potency than compounds **1** (5.585), **4** (6.004), **17** (7.131), and **19** (6.658).

The hydrogen bond donor map is displayed in Fig.8(b). There are three cyan contours, two are near substituents R2 and R3, and another small one is present at the terminal of substituent X, suggesting that hydrogen bond donor groups at these positions would increase the activity. This is in agreement with the fact that introducing electronegative groups at substituents R2 and R3 and at the terminal of substituent X would benefit the biological activity. The docking study also shows that the $-$OH and $-NH_2$ groups in these regions can form H-bonds with the carbonyl group of Glu346 or Asp463. In addition, a purple contour near substituent R1 shows an unfavorable hydrogen-bond donor interaction at this region. This is also consistent with the result that introducing a high electropositive group as substituent R1 can improve the inhibitory activity.

IV. CONCLUSION

CoMFA, CoMSIA and docking studies have been carried out on a series of pyrido[2,3-d]pyrimidine derivatives acting as Wee1 inhibitors. The established 3D-QSAR models show good correlative and predictive ability in terms of high R^2 (0.964), q^2 (0.708) for the CoMFA and R^2 (0.972), q^2 (0.645) for the CoMSIA. Meanwhile, other external validating tests further confirm the excellent predictive power of these two models. A good consistency between the 3D-QSAR contour maps and the docking results also proves the reliability and robustness of the models. Some important results can be summarized as follows: (i) The steric interaction plays a determinant role in affecting the inhibitory activities of studied derivatives. (ii) Small group and high electronegativity as substituent R2 would be advantageous to the activity, because it could not be blocked by Asp463. (iii) Moderate-size and strong electron-withdrawing group as substituent R3 could improve the activity, since it may easily result in hydrogen bond interaction with Glu346. (iv) Weak electronegativity as substituents R1 and R5 could increase the activity, because of their hydrophobic interaction with Asn431 and Ile327, respectively. (v) Moderate-size and strong hydrophilic group as substituent X would be favorable to the activity, but high electronegative atoms in the 1′-, 2′-, 3′-positions of X group could decrease the activity. These results will be helpful to understand the action mechanism and design novel potential Wee1 inhibitors.

V. ACKNOWLEDGMENTS

This work was supported by the National Natural Science Foundation of China (No.20903026), the Natural Science Foundation of Guangdong province (No.S2011010002483 and No.S2011010002964), the Science and Technology Planning Project of Guangdong Province (No.2007B030702007), and the Faculty Construction Foundation of Guangdong Pharmaceutical University. We also heartily thank the Molecular Discovery Ltd. for giving us the Dock 6.0 program as a freeware and the College of Life Sciences, Sun Yat-Sen University for the SYBYL 6.9 computation environment support.

[1] L. L. Parker and P. Worms, Science **257**, 1955 (1992).
[2] C. H. McGowan and P. Russell, EMBO J. **12**, 75 (1993).
[3] C. H. McGowan and P. Russell, EMBO J. **14**, 2166 (1995).
[4] T. Kawabe, Mol. Cancer Ther. **3**, 513 (2004).
[5] R. Heald, M. McLoughlin, and F. McKeon, Cell **74**, 463 (1993).
[6] A. Tenzer and M. Pruschy, Curr. Med. Chem. **3**, 35 (2003).
[7] J. Stumpff, T. Duncan, E. Homola, S. D. Campbell, and T. T. Su, Curr. Biol. **14**, 2143 (2004).
[8] I. Collins and M. D. Garrett, Curr. Opin. Pharmacol. **5**, 366 (2005).
[9] A. Stathis and A. Oza, Drug News Perspect **23**, 425 (2010).
[10] B. D. Palmer, A. M. Thompson, R. J. Booth, E. M. Dobrusin, A. J. Kraker, H. H. Lee, E. A. Lunney, L. H. Mitchell, D. F. Ortwine, J. B. Smaill, L. M. Swan, and W. A. Denny, J. Med. Chem. **49**, 4896 (2006).
[11] J. B. Smaill, H. H. Lee, B. D. Palmer, A. M. Thompson, C. J. Squire, E. N. Baker, R. J. Booth, A. Kraker, K. Hook, and W. A. Denny, Med. Chem. Lett. **18**, 929 (2008).
[12] J. B. Smaill, E. N. Baker, R. J. Booth, A. J. Bridges, J. M. Dickson, E. M. Dobrusin, I. Ivanovic, A. Kraker, H. H. Lee, E. A. Lunney, D. F. Ortwine, B. D. Palmer, J. Quin, C. J. Squire, A. M. Thompson, and W. A. Denny, Eur. J. Med. Chem. **43**, 1276 (2008).
[13] B. D. Palmer, J. B. Smaill, G. W. Rewcastle, E. M. Dobrusin, A. Kraker, C. W. Moore, R. W. Steinkampf, and W. A. Denny, Bioorg. Med. Chem. Lett. **15**, 1931 (2005).
[14] Y. Wang, J. Li, R. N. Booher, A. Kraker, T. Lawrence, W. R. Leopold, and Y. Sun, Cancer Res. **61**, 8211 (2001).
[15] W. J. Wu, J. C. Chen, K. C. Zheng, and F. C. Yun, Chin. J. Chem. Phys. **18**, 935 (2005).
[16] S. Y. Liao, T. F. Miao, J. C. Chen, H. L. Lu, and K. C. Zheng, Chin. J. Chem. Phys. **22**, 473 (2009).
[17] V. P. Zambre, P. R. Murumkar, R. Giridhar, and M. R. Yadav, J. Mol. Graph Model. **29**, 229 (2010).

DOI:10.1088/1674-0068/25/03/297-307

[18] J. C. Chen, L. M. Chen, S. Y. Liao, L. Qian, and K. C. Zheng, Chin. J. Chem. Phys. **22**, 285 (2009).
[19] M. D. M. AbdulHameed, A. Hamza, J. J. Liu, and C. G. Zhan, J. Chem. Inf. Model **48**, 1760 (2008).
[20] R. Thaimattam, P. R. Daga, R. Banerjee, and J. Iqbal, Bioorg. Med. Chem. **13**, 4704 (2005).
[21] J. K. Buolamwini and H. Assefa, J. Med. Chem. **45**, 841 (2002).
[22] J. C. Chen, Y. Shen, L. Qian, L. M. Chen, and K. C. Zheng, Chin. J. Chem. Phys. **20**, 135 (2007).
[23] S. Janardhan, P. Srivani, and G. N. Sastry, QSAR Comb. Sci. **25**, 860 (2006).
[24] D. Irwin, D. T. Kuntz, P. Moustakas, and L. Therese, *Dock 6.0*, University of California, (2007).
[25] *SYBYL 6.9 [CP]*, St. Louis Tripos Associates, Inc, (2001).
[26] S. J. Cho and A. Tropsha, J. Med. Chem. **38**, 1060 (1995).
[27] *Cambridge Soft Crop.*, 100 Cambridge Park, MA, 02140-2317, USA, (2010).
[28] M. J. Frish, G. W. Trucks, H. B. Schlegel, G. E. Scuseria, M. A. Robb, J. R. Cheeseman, J. A. Montgomery Jr., T. Vreven, J. C. Burant, J. M. Millam, S. S. Iyenger, J. Yomasi, V. Barone, B. Mennucci, M. Cossi, G. Scalmeni, N. Rega, G. A. Petersson, H. Nakatsuji, M. Hada, M. Ehara, K. Toyota, R. Fukuda, J. Hase-gawa, M. Ishida, T. Nakajima, Y. Honda, O. Kitao, H. Nakai, M. Klene, X. Li, J. E. Knox, H. P. Hratchian, J. B. Cross, V. Bakken, C. Adamo, J. Jaramillo, R. Gomperts, R. E. Stratmann, O. Yazyev, A. J. Austin, R. Cammi, C. Pomelli, W. Ochterski, P. Y. Ayala, K. Morokuma, G. A. Voth, P. Salvador, J. J. Dannenberg, V. G. Zakrzewski, S. Dapprich, A. D. Daniels, M. C. Strain, O. Farkas, D. K. Malick, A. D. Rabuck, K. Raghavachari, J. B. Foresman, J. V. Ortiz, Q. Cui, A. G. Baboul, S. Clifford, J. Cioslowski, B. B. Stefanov, G. Liu, A. Liashenko, P. Piskorz, I. Komaromi, R. L. Martin, D. J. Fox, T. Keith, M. A. Al-Laham, C. Y. Peng, A. Nanayakkara, M. Challacombe, P. M. W. Gill, B. Johnson, W. Chen, M. W. Wong, C. Gonzalez, and J. A. Pople, *Gaussian 03*, *Revision D.1*, CT, Wallingford: Gaussian, Inc., (2005).
[29] R. D. Cramer III, D. E. Patterson, and J. D. Bunce, J. Am. Chem. Soc. **110**, 5959 (1988).
[30] G. Klebe, U. Abraham, and T. Mietzner, J. Med. Chem. **37**, 4130 (1994).
[31] P. Geladi, Y. L. Xie, A. Polissar, and P. Hopke, J. Chemometrics **12**, 337 (1998).
[32] S. Wold, A. Ruhe, H. Wold, and W. J. Dunn, SIAM J. Sci. Stat. Comput. **5**, 735 (1984).
[33] A. Ali and J. C. Seung, Bioorg. Med. Chem. **14**, 1474 (2006).
[34] A. B. Bhoomendra, V. G. Veerappa, and K. G. Andanappa, Bioorg. Med. Chem. **13**, 2773 (2005).
[35] A. Basu, K. Jasu, V. Jayaprakash, N. Mishra, P. Ojha, and S. Bhattacharya, Eur. J. Med. Chem. **44**, 2400 (2009).
[36] P. Lu, X. Wei, and R. Zhang, Eur. J. Med. Chem. **45**, 3413 (2010).
[37] Y. L. Yan, Y. Li, S. W. Zhang, and C. Z. Ai, J. Mol. Graph Model. **29**, 747 (2011).
[38] P. P. Roy and K. Roy, QSAR Comb. Sci. **27**, 302 (2008).
[39] A. Golbraikh and A. Tropsha, J. Mol. Graph Model. **20**, 269 (2002).
[40] D. R. Roy, U. Sarkar, P. K. Chattaraj, A. Mitra, J. Padmanabhan, R. Parthasarathi, V. Subramanian, S. Van Damme, and P. Bultinck, Mol. Divers **10**, 119 (2006).

DOI:10.1088/1674-0068/25/03/297-307